Journal of Molecular Liquids 361 (2022) 119566

Contents lists available at ScienceDirect

Journal of Molecular Liquids

journal homepage: www.elsevier.com/locate/molliq

Local inversion of the mean electrostatic potential, maximum charge reversal, and capacitive compactness of concentrated 1:1 salts: The crucial role of the ionic excluded volume and ion correlations

Guillermo Iván Guerrero-García

Facultad de Ciencias de la Universidad Autónoma de San Luis Potosí, Av. Chapultepec 1570, Privadas del Pedregal, 78295 San Luis Potosí, San Luis Potosí, Mexico

ARTICLE INFO

Article history:
Received 5 January 2022
Revised 17 May 2022
Accepted 4 June 2022
Available online 8 June 2022

Keywords:
Charge inversion
Charge reversal
Capacitive compactness
Ion correlations

ABSTRACT

Recent restricted primitive model Monte Carlo simulations (Takamichi Terao, Mol. Phys. **119**, e1831634, 2020) have suggested the possibility of observing the phenomenon of charge inversion in highly concentrated monovalent salts, in which ionic specific adsorption is absent. By using the non-linear Poisson-Boltzmann equation supplemented by a hard-spheres contribution, integral equations theory, and Monte Carlo simulations, the associated mean electrostatic potential, maximum charge reversal and capacitive compactness are studied here. The main finding of this study is the observation of a local inversion of the mean electrostatic potential in a region bounded by one and three ionic radii measured from the macroions's surface. *If the zeta potential is located in this region, the above result suggests the possibility of observing an inversion of the macroion's electrophoretic mobility, driven by 1:1 aqueous electrolytes in the absence of ionic specific adsorption*. On the other hand, the maximum charge reversal and the capacitive compactness increases and decreases montonically, respectively, as a function of the ionic volume fraction when the salt concentration and/or the ionic size of the aqueous electrolytes increase.

1. Introduction

Colloidal suspensions of charged fluids are relevant in technological applications in which small charged particles are under the influence of the electric field produced by large macroions. The cloud of ions that appears around macroions in such a scenario is the so-called electrical double layer. The properties of the electrical double layer determine important physicochemical properties of charged solutions such as the corresponding colloidal stability, the flocculation behavior of the suspension and/or the effective charges of the macroions [1–3]. Experimentally, these properties can be measured via light or X-ray scattering, or via electrophoresis measurements. On the other hand, one interesting phenomenon that has been observed since the last century is the charge inversion [4], which is the inversion of roles of counterions and coions near a charged surface, that is, when charge inversion occurs it is possible to observe local spatial regions where the ionic density of coions is larger than that of counterions [5]. As a result, the net charge of a surface exposed to solution reverses polarity locally due to an excess of counterions accumulating in the immediate vicinity of the surface, which is the so-called charge reversal in colloidal systems immersed in aqueous electrolytes [5–9] or the so-called overscreening ocurring near a charged electrode next to an ionic liquid [10–12]. Charge inversion has been observed experimentally in the presence of aqueous multivalent counterions [13,14], numerically via simulations and theory of the electrical double layer of monovalent salts with different ionic radius (due, e.g., to different ionic hydration and distinct bare ionic size in general) [4,15–17], and experimentally when ionic specific adsorption is present [1,2]. In the first two instances, that is, in the absence of ionic specific adsorption, ionic excluded volume effects and ion correlations play an fundamental role in the appearance of charge inversion and charge reversal, which are not predicted by the classical non-linear Poisson-Boltzmann theory. An additional consequence of the appearance of charge inversion and charge reversal is the occurrence of a local inversion of the mean electrostatic potential near the surface of a macroion [4]. In this context, Terao has shown recently via Monte Carlo simulations [20] that there is a critical salt concentration at which the density of both coions and counterions start displaying a maximum at their closest approach distance to the macroion's surface, which is the so-called Helmholtz plane. This behaviour is not predicted by the classical non-linear Poisson-Boltzmann theory of point-ions, in which counterions tend to be in excess and coions in deficit near a colloidal charged surface due to the electrostatic attraction and repulsion between charges of different and equal signs, respectively, accord-

E-mail address: givan@uaslp.mx

https://doi.org/10.1016/j.molliq.2022.119566
0167-7322/

ing to the Coulomb law. Even more interesting it is Terao's observation of the phenomenon of charge inversion in the absence of multivalent counterions, ionic size-asymmetry in 1:1 salts, and/or ionic specific adsorption [20]. Thus, in this study it is proposed to use the non-linear Poisson-Boltzmann equation supplemented by a term representing the necessary work to bring an uncharged ion from infinite to a distance r (where r is the distance between a point in the three-dimensional space and the center of the spherical macroion), when both the macroion and the electrolyte are neutral. In such a scenario, the ionic excluded volume effects are taken into account partially even though full ion correlations are not included. A more consistent theoretical framework can be provided via integral equations theory in the Hypernetted chain/Mean spherical approximation (HNC/MSA) approach, which has been able to reproduce quantitatively and qualitatively primitive model simulations of charged systems in a wide variety of situations [4,15,17]. Thus, several theoretical approaches and Monte Carlo simulations have been used here to study the influence of the ionic excluded volume effects and ion correlations on the appearance of a critical salt concentration at which the density of both coions and counterions start displaying a maximum at the Helmholtz plane, as well as the occurrence of the phenomena of charge inversion, charge reversal, and a local inversion of the mean electrostatic potential as a function of the ionic size and the salt concentration of 1:1 aqueous electrolytes.

The remainder of this paper is organised as follows. In Section 2, the primitive model of a macroion immersed in a concentrated monovalent electrolyte is described, as well as the theoretical and simulation approaches used. In Section 3, theoretical and simulation results of the electrostatic screening at high salt concentrations and different ionic sizes are shown and discussed. Finally, in Section 4 some concluding remarks are given.

2. Model system, theories and simulations

2.1. Model system

In this study, we consider an spherical macroion with radius $R_M = 20$ Å (except in Figs. 1(d) and 1(h), where a macroion with radius $R_M = 40$ Å is also considered) and valence Z_M, immersed in a binary size-symmetric electrolyte with radius $a_+ = a_- = a$ and valence $z_+ = -z_- = 1$. An homogeneous surface charge density $\sigma_0 \leqslant 0$ is considered in all cases. As a result, counterions and coions of the bare macroion are cations and anions, respectively. The hypothesis of a constant surface charge density σ_0 is an approximation that allow us to replace the electrostatic potential produced by a charge distribution on the colloidal surface by the electrostatic potential produced by a point charge located at the macroion's center with a valence $Z_M = (\sigma_0 4\pi R_M^2)/e$, where e is the proton charge, according to Gauss's law. Experimentally, the colloidal charge is not distributed uniformly over the colloidal surface but at discrete points. However, in such a scenario, it is expected that the charge reversal, charge inversion, and the inversion of the mean electrostatic potential promoted by ion correlations be also present. The whole system is immersed in a continuum solvent with dielectric constant $\epsilon = 78.0$ at a temperature $T = 300$ K. In the presence of full ion correlations, i.e., for Monte Carlo simulations and integral equations theory in the HNC/MSA approximation, all ionic species are treated as equally-sized hard spheres with point charges in their centers, which constitute the so-called restricted primitive model. In such an approach, the interaction potential between an ion i and an ion j can be written as:

$$u_{ij}(r_{ij}) = \begin{cases} \infty, \text{if } r_{ij} < 2a, \\ \frac{z_i z_j e^2}{4\pi\varepsilon_0 \epsilon r_{ij}}, \text{if } r_{ij} \geqslant 2a, \end{cases} \tag{1}$$

where $r_{ij} = |\mathbf{r_i} - \mathbf{r_j}|$, $\mathbf{e}$ is the proton charge, and ε_0 is the vacuum permittivity. The interaction potential between the spherical macroion M and an ion j can be written as:

$$u_{Mj}(r_{Mj}) = \begin{cases} \infty, \text{if } r_{Mj} < R_M + a, \\ \\ \frac{Z_M z_j e^2}{4\pi\varepsilon_0 \epsilon r_{Mj}}, \text{if } r_{Mj} \geqslant R_M + a, \end{cases} \tag{2}$$

where $r_{Mj} = |\mathbf{r_M} - \mathbf{r_j}|$.

The primitive model incorporates ionic excluded volume effects and ion correlations in a consistent coarse grained approach. In the non-linear Poisson-Boltzmann theory ions have the same closest approach distance to the surface of the macroion, which defines the Helmholtz plane, located at $r = R_M + a$.

2.2. The non-linear Poisson-Boltzmann equation

The non-linear Poisson-Boltzmann equation for the local mean electrostatic potential can be expressed in terms of the ionic profiles next to the spherical macroion. On the other hand, the normalized ionic profile $g_i(r)$ of the species i in spherical geometry is related to the ionic potential of mean force $W_i(r)$:

$$\rho_i(r) = \rho_i^{bulk} g_i(r) = \rho_i^{bulk} e^{-W_i(r)/k_B T}, \tag{3}$$

where k_B is the Boltzmann constant and T is the absolute temperature of the system. The potential of mean force is the necessary work required to bring a charged particle from infinite to a distance r, where r is the distance between a point in the three-dimensional space and the center of the spherical macroion. As a first approximation, the potential of mean force of an ion i can be equated to the electrostatic energy $W_i(r) = e_0 z_i \Psi(r)$, where e_0 is the protonic elementary charge, z_i is the valence of the ion i and $\Psi(r)$ is the mean electrostatic potential due to the charged surface and the electrolyte. If such approximate ionic profiles, formulated in terms of the mean electrostatic potential, are substituted in the Poisson equation, $\nabla^2\Psi(r) = -\rho_{el}(r)/(\varepsilon_0\varepsilon)$, then the non-linear Poisson-Boltzmann equation is obtained

$$\nabla^2\Psi(r) = -\frac{1}{\varepsilon_0 \epsilon}\sum_i \rho_i^{bulk} z_i e_0 \exp\left(-\frac{e_0 z_i \Psi(r)}{k_B T}\right). \tag{4}$$

2.3. Hypernetted-chain/Percus-Yevick (HNC/PY) hard spheres contribution

In order to include partially ionic excluded volume effects, we propose to start with the electrostatic energy $e_0 z_i \Psi(r)$ resulting from the non-linear Poisson-Boltzmann equation (given by the Eq. 4) to add, afterwards, the potential of mean force between an ion uncharged and the macroion uncharged when each ionic species of the electrolyte is also neutral (that is, when $z_- = z_+ = Z_M = 0$), which can be written as

$$W_i^{NLPB-HNC/PY}(r) = e_0 z_i \Psi(r) + U_{HNC/PY}(r), \tag{5}$$

where $U_{HNC/PY}(r)$ is obtained as a limit case of the HNC/MSA integral equations theory as described below. This approximation is the non-linear Poisson-Boltzmann (NLPB) theory supplemented by a hard sphere contribution HNC/PY to give the NLPB-HNC/PY approximation. In the HNC/PY approximation, the ionic distribution of hard spheres is given by

$$\rho_{HNC/PY}(r) = \left[\rho_{HNC/PY}^{bulk}\right] g_{HNC/PY}(r) = \left[\rho_{HNC/PY}^{bulk}\right] e^{-U_{HNC/PY}(r)/k_B T}, \tag{6}$$

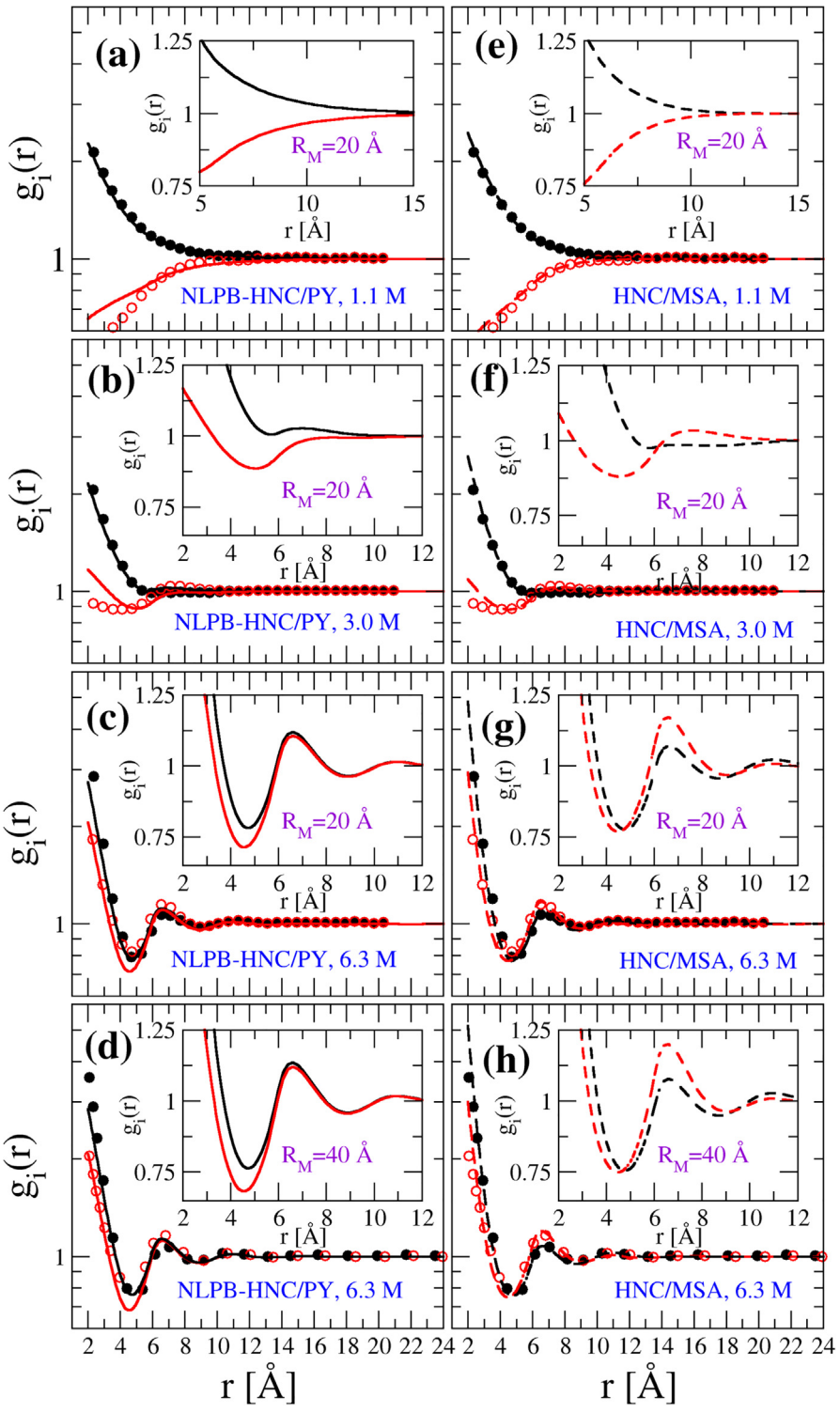

Fig. 1. Radial distribution functions of a monovalent electrolyte of radius $a = 2.0$ Å around a macroion of radius R_M for three salt concentrations: 1.1, 3.0 and 6.3 M. $Z_M = -20$ for $R_M = 20$ Å, and $Z_M = -80$ for $R_M = 40$ Å. Symbols are Monte Carlo results reported by Terao in Ref. [20], solid lines correspond to the NLPB-HNC/PY theory and dashed lines are associated to the HNC/MSA theory.

In this case, the subindex i has been dropped because all hard spheres associated to the neutral electrolyte are indistinguishable among them, and their density is measured regarding its distance to the center of the spherical uncharged colloid. Given that $g_{HNC/PY}(r) = e^{-U_{HNC/PY}(r)/k_BT}$, $U_{HNC/PY}(r)$ is calculated from integral equations theory in the presence of the macroion and the electrolyte when all species are neutral (that is, when $z_- = z_+ = Z_M = 0$) via the Ornstein-Zernike equation by using the hypernetted-chain (HNC) and Percus-Yevick (PY) closures as described in the following subsection.

Notice that the NLPB-HNC/PY prescription to include ionic excluded volume effects is analogous in spirit to one limit of the exclusion volume term function, $\zeta_{ij}(r)$, proposed by Outhwaite et al. in his Modified Poisson-Boltzmann (MPB) theory, for a binary

electrolyte modelled in the restricted primitive model [18]. Specifically, in that work it was proposed that one very simple approximation for the exclusion volume term was to equate it to the Percus-Yevick uncharged hard sphere radial distribution function, i.e., $\zeta(r) = g^{PY}(r)$. In terms of integral equations, this would correspond to solve the Ornstein-Zernike equations using the Percus-Yevick closure consistently (at the level of the direct correlation function in the Eq. 7, which discussed in the following section), in order to obtain the corresponding radial distribution function $g^{PY}(r)$ in the PY/PY approximation. In the case of a binary electrolyte, Outhwaite et al. mentioned that "At low concentrations the approximation $\zeta(r) = g^{PY}(r)$ overestimates $\zeta(r)$ near contact because of the neglect of ion correlations. However, in most situations in the electrolyte solution regime this has a negligible effect on the thermodynamic and structural properties." [18]. In this work, we study electrolyte systems in the opposite regime, that is, when the salt concentraion is high.

2.4. Integral equations theory

The Ornstein-Zernike equations describing the ionic cloud around a single spherical macroion can be written as

$$h_{Mj}(r) = c_{Mj}(r) + \sum_{k=-,+} \rho_k \int h_{Mk}(t) c_{kj}(|\vec{r} - \vec{t}|) dV, \tag{7}$$

for j = +, −, where $h_{Mj}(r)$ are the total ionic correlation functions, $g_{Mj}(r)$ are the ionic radial distribution functions, and they are related via $h_{Mj}(r) = g_{Mj}(r) - 1$. The direct correlation functions between ions and the spherical colloid are specified by using the hypernetted-chain (HNC) closure $c_{Mj}(r) = -\beta u_{Mj}(r) + h_{Mj}(r) - ln[h_{Mj}(r) + 1]$. If $c_{kj}(|\vec{r} - \vec{t}|) = -\beta(z_k z_j e_0^2)/(4\pi\varepsilon_0\epsilon|\vec{r} - \vec{t}|)$ is employed in the right-hand side of Eq. 7, the integral equations version of the non-linear Poisson-Boltzmann theory is then obtained [19]. If the $c_{kj}(|\vec{r} - \vec{t}|)$ are approximated by the bulk direct correlation functions obtained from the mean spherical approximation (MSA) then the HNC/MSA integral equations theory is obtained [4,15]. If $z_- = z_+ = Z_M = 0$ in the HNC/MSA integral equations theory, the $c_{kj}(|\vec{r} - \vec{t}|)$ are approximated by the bulk direct correlation functions obtained from the Percus-Yevick closure, that is, the HNC/PY integral equations theory for hard spheres is obtained.

2.5. Monte Carlo simulations

Monte Carlo simulations of the spherical electrical double layer have been performed in a cubic simulation box in the canonical ensemble under periodic boundary conditions. The spherical charged colloid has been placed in the center of the simulation box and has been not allowed to move. Ewald sums with conducting boundary conditions have been used to take into account correctly the long-range behaviour of Coulomb interactions. The damping constant is $\alpha = 5/L$, with L the length of the cubic simulation box. 725 vectors in the k-space have been employed to compute the reciprocal space contribution to the Coulomb energy [4,15]. If we denote N_+ and N_- as the number of cations and anions in the simulation box, respectively, the electroneutrality condition imposed in our simulations is given by $Z_M + N_+ z_+ + N_- z_- = 0$. For the equilibration process 5×10^5 Monte Carlo cycles have been performed. Between 1×10^6 and 2×10^6 Monte Carlo cycles have been carried out to calculate the canonical average of the systems, depending on the electrolyte concentration. Notice that in the work performed by Terao [20] isotropic approximations to Ewald sums based on Kubic Harmonics have been used to take into account properly long-range electrostatic interactions, whereas full Ewald sums were performed in this work. Monte Carlo simulations in Terao's work and in this study seem to be equivalent according to the data displayed in Figs. 2 and 4. Some details regarding typical running times, total number of charged particles, and absence of size effects due to the size of the simulation box are discussed in the Supplementary Material.

2.6. Some electrostatic properties of the electrical double layer in spherical geometry

The integrated charge, electric field, and mean electrostatic potential can be written for the NLPB-HNC/PY and HNC/MSA integral equations theories, and Monte Carlo simulations as [23]

$$P(r) = Z_M + \sum_{i=+,-} \int_0^r z_i \rho_i^{bulk} g_{Mi}(t) 4\pi t^2 dt, \tag{8}$$

$$E(r) = \frac{e_0}{4\pi\varepsilon_0\epsilon} \frac{P(r)}{r^2}, \tag{9}$$

$$\Psi(r) = \int_r^\infty E(t) dt. \tag{10}$$

Another useful quantity to characterize the thickness of the electrical double layer is the *capacitive compactness*. This idea was proposed by Enrique Gonzalez-Tovar in 2004 to explain an anomalous curvature inversion of the mean electrostatic potential observed at the Helmholtz plane of a spherical macroion, as a function of its colloidal surface charge density, when the macroion was bathed by a 1:1 or a 2:2 size-symmetric aqueous electrolyte [22]. Since then, the capacitive compatcness has proven to be a versatile concept that allow us to characterize the spatial extension of the electrical double layer in charged soft condensed matter systems [21,23–27]. The main idea behind the capacitive compactness is to define an effective electrical double layer capacitor associated to a single charged colloidal particle neutralized by a Coulombic fluid. In such a scenario, the separation distance between the real electrode (associated to the charged colloidal particle) and the effective electrical double layer electrode (associated to the *centroid* of the diffuse ionic charge) is the so-called capacitive compactness [21,23]. In the limit of zero colloidal charge, the capacitive compactness measured from the Helmholtz plane reduces to the Debye length according to the linearized Poisson-Boltzmann or Debye-Hückel theory of point-ions, in planar and spherical geometries [23,27]:

$$\tau_c^{DH} = \frac{1}{\kappa_D} = \lambda_D, \tag{11}$$

where

$$\kappa_D = \left(\frac{\sum_i \rho_i^{bulk} z_i^2 e_0^2}{\varepsilon_0 \epsilon k_B T} \right)^{\frac{1}{2}} = \frac{1}{\lambda_D}, \tag{12}$$

and λ_D is the Debye length. As a result, and according to this formalism, the capacitive compactness is always located beyond the Helmholtz plane given that κ_D is always a positive quantity if the concentration of the electrolyte is different from zero. One advantage of the capacitive compactness over the Debye length is that the former allow us to include important characteristics typical of Coulombic fluids, such as the colloidal charge, ionic excluded volume effects, ion correlations, image charge or polarization effects, specific ionic adsorption, etc. In spherical geometry, the capacitive compactness is defined as [22,27]:

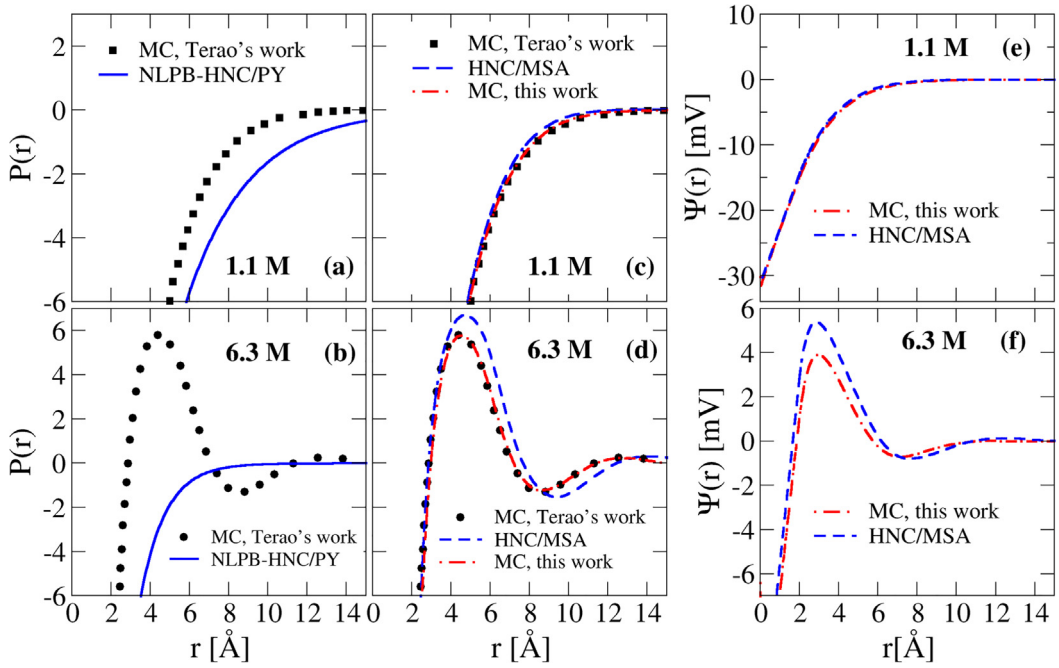

Fig. 2. Integrated charge and mean electrostatic potential associated to a monovalent electrolyte of radius $a = 2.0$ Å around a macroion of valence $Z_M = -20$ and radius $R_M = 20$ Å. Symbols are Monte Carlo results reported by Terao in Ref. [20], solid lines correspond to the NLPB-HNC/PY theory, dashed lines are associated to the HNC/MSA theory, and dot-dashed lines correspond to Monte Carlo simulations performed in this work.

$$\tau_c = \left(\frac{1}{R_M} - 4\pi\varepsilon_0\epsilon\frac{\Psi_0}{e_0 Z_M}\right)^{-1}, \tag{13}$$

where Ψ_0 is the mean electrostatic potential at the macroion's surface, i.e., at $r = R_M$.

Integral equations theory has been solved using an efficient iterative Picard scheme [16], which allowed us to generate the NLPB-PY and HNC/MSA results.

Note that at high electrolyte concentrations, the non-linear Poisson-Boltzmann theory break-downs because allows to adsorb an arbitrary number of counterions on the colloidal surface. One of the most simple routes to overcome this problem has been to include the entropy associated to the ions and the solvent, which constitutes the so-called Bikermann model [28]. Other approaches have been proposed to connect the equation of state for any reference uncharged fluid (such as the Carnahan-Starling or the Boublík-Mansoori-Carnahan-Starling-Leland state equations for hard spheres) with the non-linear Poisson-Boltzmann theory, keeping the electrostatics at a mean-field level but taking into account consistently the packing effects [29]. The proposed NLPB-HNC/PY theory is at the same level of these previous theories, in which the ionic excluded volume effects are effectively incorporated via a state equation at the level of Percus-Yevick. In spite of their simplicity, these mean field approaches have been able to predict the parabolic to camel-shape transition of the differential capacity, which is absent in the classical non-linear Poisson-Boltzmann theory. Another successful mean-field treatment that has been proposed in recent years in the context of ionic liquids is one based on a Landau-Ginzburg-like functional for the total free energy [10], which is able to predict the phenomenon of charge reversal or overscreening. Recently, this approach has been connected to the Carnahan-Starling equation of state, displaying a good qualitative agreement regarding repulsive-core primitive model simulations [11]. Thus, this last theory seems to be equally predictive regarding the HNC/MSA integral equations, considering that both schemes are able to predict charge inversion and charge reversal due to ion correlations and ionic excluded volume effects.

3. Results and discussion

In Fig. 1, the radial distribution functions predicted by Monte Carlo simulations [20] are collated with data obtained from the NLPB-HNC/PY and HNC/MSA integral equation theories for several salt concentrations. Here, it is observed that the NLPB-HNC/PY approximation, which does not include ion correlations, it was able to display the maxima predicted by Monte Carlo simulations of both coions and counterions at the closest approach distance between ions and the macroion's surface, or Helmholtz plane, as well as the appearance of oscillations of the radial distribution functions. These oscillations become more conspicuous when the bulk salt concentration increases (see, e.g., Figs. 1(a)-(c)). On the other hand, it is observed that the NLPB-HNC/PY approximation has failed to display the charge inversion, or the role inversion of cations as counterions and coions as anions, predicted by Monte Carlo simulations. This illustrates that even though ionic excluded volume effects are very relevant to predict maxima for the radial distribution functions of both coions and counterions at the Helmholtz plane, as well as ionic density oscillations, the absence of charge inversion in the NLPB-HNC/PY confirms that ion correlations are crucial to the occurrence of this phenomenon if equally sized monovalent ions are present. On the other hand, HNC/MSA integral equations theory exhibits a qualitative agreement regarding Monte Carlo simulations, displaying maxima for the radial distribution functions of both coions and counterions at the Helmholtz plane, ionic density oscillations, and charge inversion. Note that the oscillatory behaviour of the ionic profiles in concentrated electrolyte solutions originates from the competition between local packing effects and long-range Coulomb interactions, as it has been documented in previous works, see, e.g., Refs. [30–33]. On the other side, the maxima of the radial distribution functions of both coions and counterions at the Helmholtz and

the charge inversion are enhanced if the macroion radius increases, as shown in Figs. 1(g)-(h), according to Monte Carlo simulations and the HNC/MSA integral equations theory.

In Figs. 2(a)-(d), the integrated charge associated to Monte Carlo simulations and data obtained from the NLPB-HNC/PY and HNC/MSA integral equation theories is portrayed. Here, it is seen that the HNC/MSA integral equation data display a good agreement regarding Monte Carlo simulations showing the phenomenon of charge reversal, which is the sign inversion of the local integrated charge regarding the sign of the macroion's bare charge. The absence of charge reversal associated to the NLPB-HNC/PY data is consistent with the lack of charge inversion displayed in Figs. 1(-a)-(d) in all instances. In Figs. 2(e)-(f), the mean electrostatic potential curves associated to Figs. 2(c)-(d), respectively, are displayed. Here, Monte Carlo simulations show a local inversion of the mean electrostatic potential in a spatial region bounded by one and three ionic radii measured from the macroion's surface, that is, $R_M + a \leqslant r \leqslant R_M + 3a$ approximately. This behaviour is also predicted by the HNC/MSA integral equations theory, displaying a semi-quantitative agreement with Monte Carlo data. The charge reversal and the mean electrostatic potential are slightly overestimated by the HNC/MSA integral equation data.

The mean electrostatic potential at the Helmholtz plane, ψ_H, is conventionally associated to the zeta potential [1,2], which is defined as the mean electrostatic potential at the slipping plane in electrophoresis experiments. The exact location of the zeta potential at the slipping plane is not known usually a priori from first principles. However, it is known that it is located generally very close to the colloidal surface. Therefore, from the above results, if the experimental zeta potential is located between the Helmholtz plane and three ionic radii measured from the macroions's surface, *a local inversion of the mean electrostatic potential suggests the possibility of observing an inversion of the macroion's electrophoretic mobility, driven by highly concentrated 1:1 aqueous electrolytes in the absence of ionic specific adsorption.*

In Fig. 3, the behaviour of the mean electrostatic potential at the Helmholtz plane ψ_H, as a function of the ionic radius and the salt concentration, is displayed according to Monte Carlo simulations and HNC/MSA integral equations theory. Here, it is observed that the sign of ψ_H changes from a negative value (that is the sign associated to the bare charge of the macroion) to a positive value for several ionic radius at very high salt concentrations. In this regime, it is possible to observe an augment of the magnitude of the inverted mean electrostatic potential at the Helmholtz plane as a function of the ionic radius in concentrated salts. Thus, the local inversion of the mean electrostatic potential at the Helmholtz plane is promoted by the augment of the ionic volume fraction when ion correlations are present.

The location of the slipping plane depends on many factors such as the chemical composition of the colloidal surface, the hydrophobicity or hydrophilicity of ions, the specific ionic adsorption, etc. In the current model, these features are not included. However, it is foreseen that they should enhance the charge reversal, charge inversion, and the inversion of the mean electrostatic potential promoted by ion correlations and ionic excluded volume effects already observed in the minimalistic primitive model used. From a numerical point of view, an equilibrium theoretical approach that be able to capture charge reversal or overscreening [10–12] is suitable to be used in the methodology proposed by Stout and Khair [34], which incorporates hydration forces, or other methodologies that also take into account ionic relaxation effects [35,36]. In order to test the inversion of the electrophoretic mobility experimentally, it is necessary to use aqueous electrolytes that do not experience specific ionic adsorption regarding the colloidal surface, and that be soluble at high salt concentrations, such as NaCl, KCl, LiCl, RbCl etc. [37]. For simplicity, equally-sized ions have been consid-

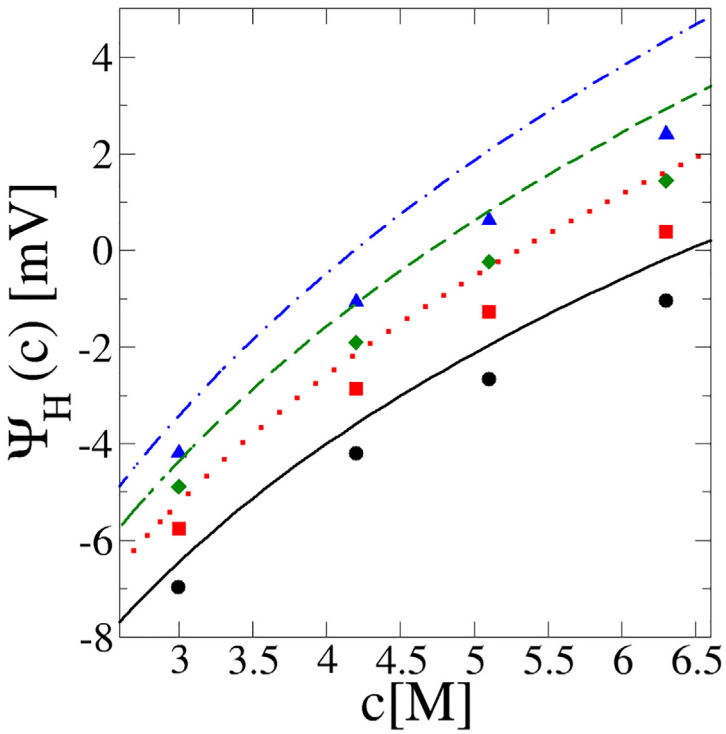

Fig. 3. Mean electrostatic potential at the Helmholtz plane located at $r_H = R_M + a$, as a function of the salt concentration and the ionic radius. The valence and radius of the macroion are $Z_M = -20$ and $R_M = 20$ Å, respectively. Symbols and lines correspond to Monte Carlo simulations and HNC/MSA theoretical calculations performed in this work. The statistical uncertainties of Monte Carlo simulation results are smaller than the symbol size. Black, red, green, and blue symbols and lines are associated to a ionic radius 1.75, 1.9. 2.0 and 2.1 Å, respectively.

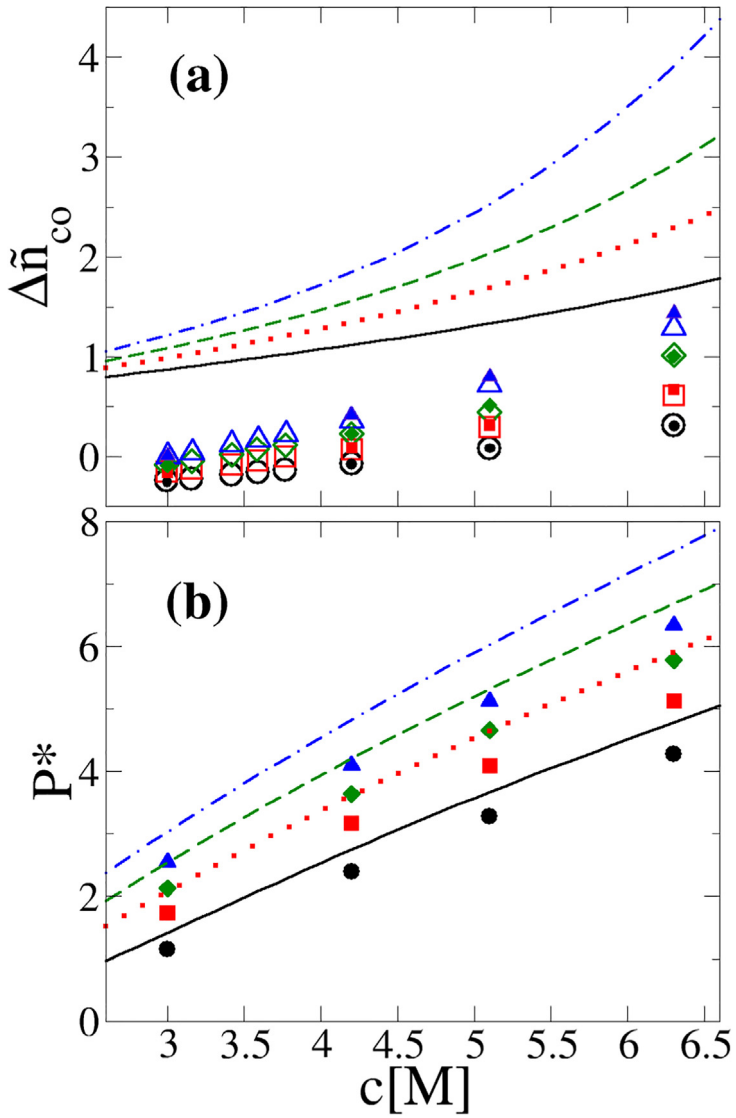

Fig. 4. (a) Dimensionless excess coion density and (b) maximum integrated charge as a function of the salt concentration and the ionic radius. The valence and radius of the macroion are $Z_M = -20$ and $R_M = 20$ Å, respectively. Symbols and lines correspond to Monte Carlo simulations and HNC/MSA theoretical calculations performed in this work. The statistical uncertainties of Monte Carlo simulation results are smaller than the symbol size. Black, red, green, and blue symbols and lines are associated to an ionic radius 1.75, 1.9. 2.0 and 2.1 Å, respectively. In panel (a), empty symbols correspond to Monte Carlo simulations reported by Terao in Ref. [20]. Solid symbols in panels (a) and (b) correspond to Monte Carlo data performed in this work.

ered in this work. However, in nature, ions are usually size-asymmetric due to different degrees of solvation and different bare ionic sizes. Electrolytes in which counterions are smaller than coions have shown to promote like charge attraction between equally charged macroions via an ion-bridging mechanism, in the absence of ionic specific adsorption [38]. Thus, this size-combination for counterions and coions seems to be appropriate to test experimentally the proposed inversion of the electrophoretic mobility in the presence of indifferent monovalent electrolytes, that is, in the presence of monovalent ions that do not experience specific adsorption regarding the colloidal surface. In addition to the inversion of the electrophoretic mobility, it would be very interesting to study the behaviour of the effective charge when the mean electrostatic potential inverts. In such a scenario, it would be necessary to calculate the radial distribution function of macroions at finite concentration via simulations and theory, in order to determine the role of the macroion-macroion correlations. In previous works, it has been shown that charged colloids at finite concentration can display a macroion shielding, which affects the microion distribution around a macroion and the thermodynamic stability of the whole dispersion [39].

Let us define the dimensionless excess coion density, or total correlation function at the Helmholtz plane, as [20]

$$\Delta\tilde{n}_{co} = h_{M,-1}(r = R_M + a_-) = g_{M,-1}(r = R_M + a_-) - 1. \quad (14)$$

and the maximum charge reversal as $P^* = P(r = r^*) \geqslant P(r)$ for all r, where r^* is the location of the maximum charge reversal. The dimensionless excess coion density $\Delta\tilde{n}_{co}$ and the maximum charge reversal P^* obtained via Monte Carlo simulations and the HNC/MSA integral equation theory are displayed in Figs. 4(a) and 4(b), respectively, for several ionic radius and salt concentrations. Here, it is noted that both quantities show a similar monotonic behavior, that is, for a fixed ionic size both quantities increase as a function of the ionic concentration, and for a fixed ionic concentration they augment when the ionic size increases. Thus, $\Delta\tilde{n}_{co}$ and P^* increase monotonically as a function of the ionic volume fraction. Even though the contact values of coions are overestimated by HNC/MSA regarding Monte Carlo data, the theoretical maximum charge

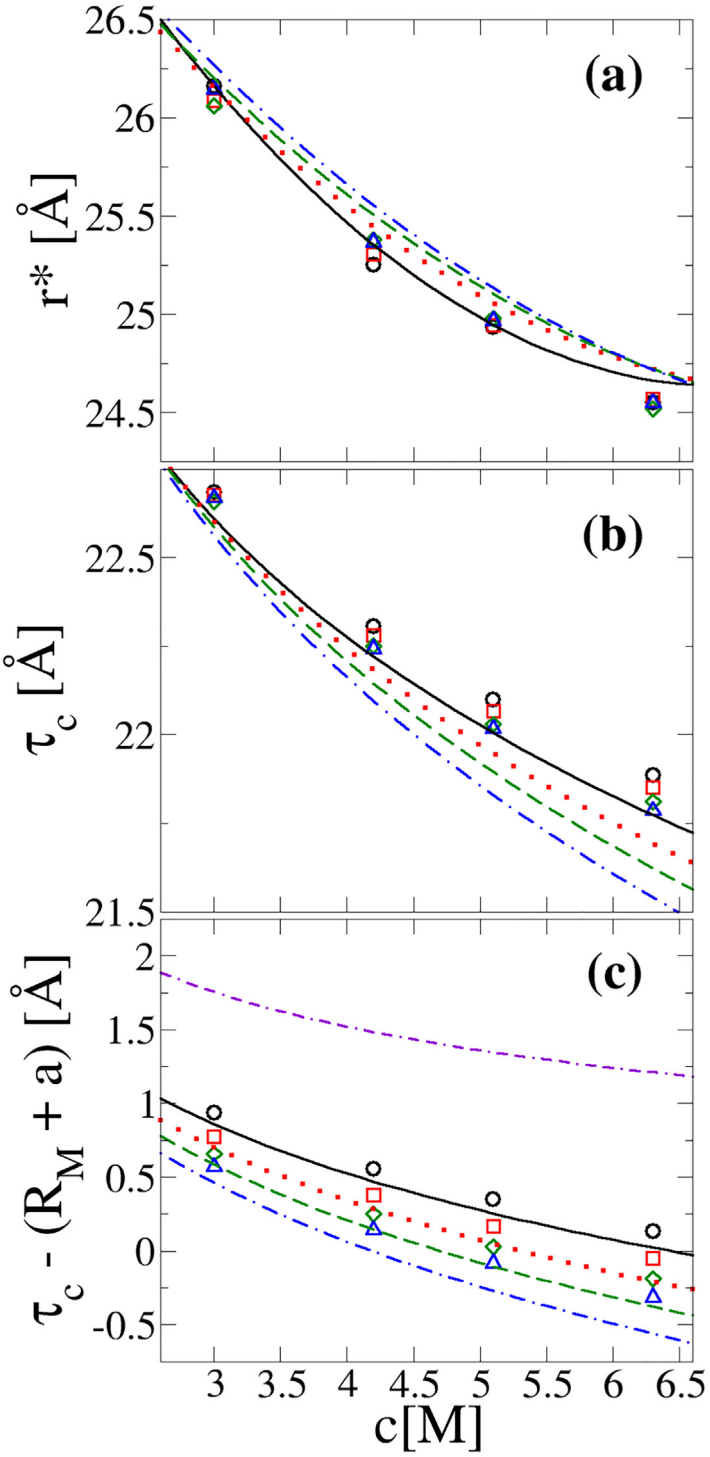

Fig. 5. Location of (a) the maximum integrated charge and (b) the capacitive compactness measured from the center of the macroion as a function of the salt concentration and the ionic radius. In the panel (c), the capacitive compactness is measured from the Helmholtz plane located at $r_H = R_M + a$. The valence and radius of the macroion are $Z_M = -20$ and $R_M = 20$ Å, respectively. Symbols and lines correspond to Monte Carlo simulations and HNC/MSA theoretical calculations performed in this work. The statistical uncertainties of Monte Carlo simulation results are smaller than the symbol size. Black, red, green, and blue symbols and lines are associated to an ionic radius 1.75, 1.9. 2.0 and 2.1 Å, respectively. In panel (c), the dot-double dashed purple line corresponds to the Debye length as function of the concentration.

reversal is close to the simulation results. In both instances, HNC/MSA data display the same trend shown by the Monte Carlo simulations.

In order to characterize the thickness of the electrical double layer, in Fig. 5 are plotted the location of the maximum charge reversal P^* measured from the macroion's center r^* (Fig. 5(a)), as well as the capacitive compactness τ_c measured from the macroion's center (Fig. 5)) and from the ionic closest approach distance or Helmholtz plane (Fig. 5(c)). In this instance, it is observed that r^* and τ_c decrease when the ionic volume fraction increases, for instance, when the ionic concentration augments for a fixed ionic size or when the ionic size increases for a fixed ionic concentration. This means that the electrical double layer shrinks or becomes more compact when the ionic volume fraction increases. In this

case, monovalent counterions can overcompensate the bare charge of the macroion and this, in turn, promotes the appearance of regions where charge inversion appears close to the macroion's surface, in order to fulfill the global electroneutrality condition. When the ionic volume fraction further increases, the ionic excluded volume promotes higher contact values of coions and counterions and the appearance of spatial oscillations, as it has been shown in Figs. 1(e)-(h). When the electrical double layer shrinks at very high salt concentrations, the local overcompensation of the bare charge increases and, as a result, the maximum charge reversal exacerbates due to ion correlations as it has been illustrated in Figs. 1(e)-(h) and 4(b).

On the other hand, in Fig. 5(b) it is seen that the capacitive compactness measured from the center of the macroion is always larger than R_M. According to the linearized Poisson-Boltzmann or Debye-Hückel theory of point-ions in planar and spherical geometries [23], the capacitive compactness measured from the Helmholtz plane reduces to the bulk Debye length for any colloidal charge. As a result, this mean-field approach predicts that the capacitive compactness is always positive if it is measured from the Helmholtz plane for electrolytes with non-zero concentration. In Fig. 5(c), the capacitive compactness measured from the Helmholtz plane is displayed. Here, it is observed that there is a critical concentration at which the capacitive compactness becomes negative according to Monte Carlo simulations and the HNC/MSA integral equations theory. This means that the electrical double layer becomes so compact that the separation distance between the electrodes of the associated effective spherical capacitor can be smaller than an ionic radius *a*. Such a behaviour constrasts with the linearized Poisson-Boltzmann or Debye-Hückel picture, in which the separation distance between the electrodes of the associated effective spherical capacitor is $a + \lambda_D$. On the other hand, notice that even though the Debye length decreases when the numerical ion concentration augments, this quantity, by definition, is not able to take into account the ionic size or the ionic volume fraction.

4. Conclusions

In this work, we have proposed to include partially ionic excluded volume effects on top of the mean field electrostatic energy obtained from the non-linear Poisson Boltzmann equation to give the NLPB-HNC/PY approximation. Even though this approximation does not include ion correlations, it was able to predict that, at high salt concentrations, the density of both coions and counterions can show a maximum at the Helmholtz plane, as well as the appearance of ionic density oscillations similar to those predicted by Monte Carlo simulations [20]. In spite of this qualitative agreement, the NLPB-HNC/PY approximation has failed to display the charge inversion shown by Monte Carlo simulations and HNC/MSA integral equations theory, where ion correlations are included consistently. This confirms that ion correlations are fundamental to the appearance of charge inversion in 1:1 aqueous electrolytes in the absence of ionic specific adsorption. On the other hand, HNC/MSA integral equations theory has displayed a good qualitative and semi-quantitative agreement regarding Monte Carlo simulations, i.e., this theoretical approach has been able to show that, at high ionic volume fractions, i) the density of both coions and counterions can display a maximum the Helmholtz plane, ii) the appearance of the phenomena of charge inversion, charge reversal, and a local inversion of the mean electrostatic potential near the surface of the colloid, and iii) the augment of the dimensionless excess coion density and the maximum charge reversal when the ionic volume fraction increases.

More importantly, it has been shown that it is possible to observe a local inversion of the mean electrostatic potential in a region bounded by one (i.e., at the Helmholtz plane) and three ionic radii measured from the macroions's surface. The mean electrostatic potential at the Helmholtz plane is conventionally associated to the zeta potential, which is the mean electrostatic potential at the slipping plane. *If the zeta potential is located in the above indicated region, a local inversion of the mean electrostatic potential suggests the possibility of observing an inversion of the macroion's electrophoretic mobility, driven by indiferent 1:1 aqueous electrolytes*, analogous to that observed in the presence of aqueous multivalent counterions and/or ionic specific adsorption [40,41].

On the other hand, it has been shown that the location of the maximum charge reversal and the capacitive compactness decreases when the ionic volume fraction increases, which suggests that the electrical double layer shrinks or becomes more compact under these conditions. Moreover, it has been seen that there is a critical concentration at which the capacitive compactness, measured from Helmholtz plane, becomes negative. This means that the electrical double layer becomes so compact that the separation distance between the electrodes of the associated effective spherical capacitor can be smaller than an ionic radius *a*. Such a behaviour constrasts with the linearized Poisson-Boltzmann or Debye-Hückel picture, in which the separation distance between the electrodes of the associated effective spherical capacitor is $a + \lambda_D$.

It would be very interesting to calculate the electrophoretic mobility [35,36] associated to the systems studied in this work, in order to corroborate the possibility of an inversion of the colloidal mobility driven by monovalent salts, in the absence of ionic specific adsorption, at very high salt concentrations. Work in this direction is in progress and it will be published elsewhere.

Declaration of Competing Interest

The authors declare the following financial interests/personal relationships which may be considered as potential competing interests: Guillermo Ivan Guerrero Garcia reports financial support was provided by National Research Council of Science and Technology, Mexico. Guillermo Ivan Guerrero Garcia reports financial support was provided by Autonomous University of San Luis Potosi.

Acknowledgements

G. I. G.-G. acknowledges the SEP-CONACYT grants CB-2016-286105 and FOP16-2021-01-320091, the 2019 Marcos Moshinsky Fellowship, the National Supercomputing Center-IPICYT for the computational resources provided via the grant TKII-IVGU001, and the computing time granted by LANCAD and CONACYT in the Supercomputer Hybrid Cluster "Xiuhcoatl" at GENERAL COORDINATION OF INFORMATION AND COMMUNICATIONS TECHNOLOGIES (CGSTIC) of CINVESTAV with the project 58-2021. The author thanks the anonymous Reviewers for their useful comments and constructive suggestions, thanks Prof. Enrique González-Tovar for providing insightful suggestions and proofreading the manuscript, and expresses his gratitude for the assistance from the computer technicians at the IF-UASLP.

Appendix A. Supplementary material

Supplementary data associated with this article can be found, in the online version, at https://doi.org/10.1016/j.molliq.2022.119566.

References

[1] R.J. Hunter, Zeta Potential in Colloid Science, Academic Press, New York, 1981.
[2] R.J. Hunter, Foundations of Colloid Science, Clarendon, Oxford, 1987.
[3] W.B. Russell, D.A. Saville, W.R. Schowalter, Colloidal Dispersions, Cambridge University Press, Cambridge, UK, 1989.
[4] G.I. Guerrero-García, E. González-Tovar, M. Olvera de la Cruz, Soft Matter 6 (2010) 2056–2065.
[5] H. Greberg, R. Kjellander, J. Chem. Phys. 108 (1998) 2940.
[6] L.B. Bhuiyan, C.W. Outhwaite, D. Henderson, J. Chem. Eng. Data 56 (2011) 4556–4563.
[7] A. Voukadinova, M. Valiskó, D. Gillespie, Phys. Rev. E 98 (2018) 012116.
[8] L.B. Bhuiyan, L. Blum, D. Henderson, J. Chem. Phys. 78 (1983) 442.
[9] A.P. dos Santos, M. Girotto, Y. Levin, J. Chem. Phys. 144 (2016) 144103.
[10] M.Z. Bazant, B.D. Storey, A.A. Kornyshev, Phys. Rev. Lett. 106 (2011) 046102.
[11] J.P. de Souza, Z.A.H. Goodwin, M. McEldrew, A.A. Kornyshev, M.Z. Bazant, Phys. Rev. Lett. 125 (2020) 116001.
[12] R.P. Misra, J.P. de Souza, D. Blankschtein, M.Z. Bazant, Langmuir 35 (2019) 11550–11565.
[13] K. Besteman, M.A.G. Zevenbergen, H.A. Heering, S.G. Lemay, Phys. Rev. Lett. 93 (2004) 170802.
[14] F.H.J. van der Heyden, D. Stein, K. Besteman, S.G. Lemay, C. Dekker, Phys. Rev. Lett. 96 (2006) 224502.
[15] G.I. Guerrero-García, E. González-Tovar, M.O. de la Cruz, J. Chem. Phys. 135 (2011) 054701.
[16] G.I. Guerrero-García, M.O. de la Cruz, J. Phys. Chem. B 118 (2011) 8854–8862.
[17] G.I. Guerrero-García, Biophys. Chem. 282 (2022) 106747.
[18] L.B. Bhuiyan, C.W. Outhwaite, M. Molero, E. González-Tovar, J. Chem. Phys. 100 (1994) 8301.
[19] E.A. Barrios-Contreras, E. González-Tovar, G.I. Guerrero-García, Mol. Phys. 113 (2015) 1190–1205.
[20] T. Terao, Mol. Phys. 10 (2020) e1831634.
[21] G.I. Guerrero-García, E. González-Tovar, M. Chávez-Páez, J. Kłos, S. Lamperski, Phys. Chem. Chem. Phys. 20 (2018) 262–275.
[22] E. González-Tovar, F. Jiménez-Ángeles, René Messina, M. Lozada-Cassou, J. Chem. Phys. 120 (2004) 9782.
[23] G.I. Guerrero-García, E. González-Tovar, M. Chávez-Páez, Tao Wei, J. Mol. Liq. 277 (2019) 104–114.
[24] C.L. Moraila-Martínez, G.I. Guerrero-García, M. Chávez-Páez, E. González-Tovar, J. Kłos, J. Chem. Phys. 148 (2018) 154703.
[25] C.N. Patra, RSC Adv. 10 (2020) 39017–39025.
[26] J.J. Elisea-Espinoza, E. González-Tovar, J.A. Martínez-González, C.G. Galván Peña, G.I. Guerrero-García, Mol. Phys. 119 (2021) e1916633.
[27] E. González-Tovar, J.A. Martínez-González, C.G. Galván Peña, G.I. Guerrero-García, J. Chem. Phys. 154 (2021) 096101.
[28] I. Borukhov, D. Andelman, H. Orland, Phys. Rev. Lett. 79 (1997) 435–438.
[29] A.C. Maggs, R. Podgornik, Soft Matter 12 (2016) 1219–1229.
[30] J.G. Kirkwood, J.C. Poirier, J. Phys. Chem. 58 (1954) 591–596.
[31] F.H. Stillinger Jr., R. Lovett, J. Chem. Phys. 49 (1968) 1991.
[32] J.-P. Hansen, I.R. McDonald, Theory of Simple Liquids, Academic Press, London, 1986.
[33] C.W. Outhwaite, M. Molero, L.B. Bhuiyan, J. Chem. Soc., Faraday Trans. 87 (1991) 3227.
[34] R.F. Stout, A.S. Khair, J. Fluid Mech. 752 (2014) R1.
[35] C. Contreras Aburto, G. Nägele, J. Chem. Phys. 139 (2013) 134109.
[36] C. Contreras Aburto, G. Nägele, J. Chem. Phys. 139 (2013) 134110.
[37] W.M. Haynes, Editor-in-Chief, CRC Handbook of Chemistry and Physics, 97th Edition., CRC Press, Boca Raton FL, 2017.
[38] G.I. Guerrero-García, P. González-Mozuelos, M. Olvera de la Cruz, J. Chem. Phys. 135 (2011) 164705.
[39] R. Klein, H.H. von Grunberg, C. Bechinger, M. Brunner, V. Lobaskin, J. Phys.: Condens. Matter 14 (2002) 7631–7648.
[40] M. Elimelech, C.R. O'Melia, Colloids Surf. 44 (1990) 165–178.
[41] I. Semenov, S. Raafatnia, M. Sega, V. Lobaskin, C. Holm, F. Kremer, Phys. Rev. E 87 (2013) 022302.